INLETS, DUCTS, AND NOZZLES

John M. Abbott,
Bernhard H. Anderson,
and Edward J. Rice

SUMMARY

The internal fluid mechanics research program in inlets, ducts, and nozzles consists of a balanced effort between the development of computational tools (both parabolized Navier-Stokes and full Navier-Stokes) and the conduct of experimental research. The experiments are designed to better understand the fluid flow physics, to develop new or improved flow models, and to provide benchmark quality data sets for validation of the computational methods.

The inlet, duct, and nozzle research program is described according to three major classifications of flow phenomena: (1) highly three-dimensional flow fields, (2) shock - boundary-layer interactions, and (3) shear layer control. Specific examples of current and future elements of the research program are described for each of these phenomenon. In particular, the highly three-dimensional flow field phenomenon is highlighted by describing the computational and experimental research program in transition ducts having a round-to-rectangular area variation. In the case of shock - boundary-layer interactions, the specific details of research for normal shock - boundary-layer interactions are described. For shear layer control, research in vortex generators and the use of aerodynamic excitation for enhancement of the jet mixing process are described.

Future research in inlets, ducts, and nozzles will include more emphasis on three-dimensional full Navier-Stokes methods and corresponding experiments designed to concentrate on the appropriate three-dimensional fluid flow physics.

INTRODUCTION

The internal fluid mechanics research program in inlets, ducts, and nozzles is described according to three types of fluid flow phenomena: highly three-dimensional flow fields, shock - boundary-layer interactions, and shear layer control. The importance of each of these flow phenomena is a result of the drivers listed in figure 1. For example, highly three-dimensional internal flow fields result from unconventional engine locations where twisting and turning inlets, ducts, and nozzles must be designed to deliver the airflow to and from the free stream. Aircraft thrust vectoring requirements quite often lead to the transitioning of nozzle cross-sectional geometries from round to rectangular with resultant three-dimensional flows. Aircraft maneuverability requirements can lead to significant three-dimensional flow fields entering

the propulsion system inlet and ducting system. The push toward higher flight speeds, for both military and civilian applications, leads to the importance of research in shock - boundary-layer interactions within inlets, ducts, and nozzles. The desire to design inlets, ducts, and nozzles to be as short and light as possible points to the importance of shear layer control as a means for "stretching" the limits of the geometry while avoiding internal flow separations. Shear layer control in another sense, that is, the use of aerodynamic excitation to control the formation and development of a mixing layer, offers the potential for enhancing the mixing process in external nozzle flows.

Specific elements of the inlet, duct, and nozzle research program are listed in figure 2 for each of the three flow field phenomena. The four elements underlined in the figure will be expanded upon in the remainder of the paper. Specifically, highly three-dimensional flow fields will be illustrated by describing the transition duct research program. The shock - boundary-layer interaction phenomenon will be illustrated with a description of the normal shock - boundary-layer interaction research program. Shear layer control research will be illustrated with two examples of current programs: vortex generator research and enhanced jet mixing research. The remaining four elements of the overall program, that is, offset ducts, oblique shock - boundary-layer interactions, glancing sidewall shock - boundary-layer interactions, and boundary-layer bleed, will not be described in this paper, although they are also key elements of the overall program.

As illustrated in figure 3, the approach to the research program in inlets, ducts, and nozzles consists of a balance between computational and experimental research. Computationally, much of the emphasis up until recently has been on the development and validation of parabolized Navier-Stokes methods. More recently and for the future, more emphasis is being placed on three-dimensional full Navier-Stokes methods. Shown on the right-hand side of the figure are the elements of the experimental program in inlets, ducts, and nozzles. They are aligned with the respective computational method and point out the close linkage between the computational and experimental elements of the program. Note that each of the program elements listed in figure 2 under the three different flow phenomena also appear here in figure 3 as specific experiments.

HIGHLY THREE-DIMENSIONAL FLOW FIELDS

Transition Ducts

Highly three-dimensional flow field research is illustrated by describing the transition duct research program.

Transition ducts are characterized by a cross-sectional geometry that transitions from round to rectangular (ref. 1). A sample three-dimensional parabolized Navier-Stokes (PNS) computation for a specific transition duct geometry is illustrated in figure 4. (Details of the computational method are given in refs. 2 and 3.) The geometry is described by a rectangular exit having an aspect ratio (width/height) of 3.0. The duct is 1.5 inlet diameters long and has an exit-to-inlet area ratio of 1.0. The figure shows near-wall velocity vectors on the left, with a display of the secondary velocity vectors in the rectangular exit plane shown below it. The three-dimensional character of

the flow field is clear. On the right side of the figure are contours of surface shear stress on the duct. Zero shear stress corresponds to the onset of flow separation on the duct surface. Note that the computation indicates that this particular geometry has a small localized separation zone about halfway down the duct. The flow reattaches just downstream of this zone and remains attached for the remainder of the duct length. The separation is apparent in both the near-wall velocity vectors and in the surface shear stress contours.

As an illustration of how the computational results shown in the previous figure can be used, figure 5 shows the internal flow separation bounds for a class of transition duct geometries. Each duct geometry has the same area ratio of 1.0, but the length ratio and the exit aspect ratio are varied. Specifically, for four different aspect ratios, the length ratio was decreased from a value where the internal flow was completely attached to a value where the flow just began to separate. This series of computations then resulted in the separation bound shown in the figure. For geometries above the curve, the flow is attached; for geometries below the curve, the flow is separated. One experimental data point is spotted on the figure as a case where the flow was massively separated within the duct.

To develop a more detailed understanding of the flow physics within transition ducts, to improve models of the flow physics, and to validate computations like those shown in the previous two figures, experiments are underway using the model and facility shown in figure 6. The model was machined to match exactly one of the geometries for which the three-dimensional PNS method had been applied. Shown in this figure is a photo of the model during the final machining stage together with a superimposed display of the computational surface. Also shown is the test facility. Special care was taken to condition the transition duct inflow properly to provide the desired levels of inflow turbulence, flow angularity, and boundary-layer profile. Modifications to the facility are currently underway whereby the inflow tank is being connected to a high-pressure supply system to provide higher Reynolds number test capability.

Experimental results are shown in figure 7 at a one-dimensional duct Mach number of 0.5. On the left side of the figure, surface static pressure measurements are shown along the centerline of the duct. On the right side of the figure are shown results from a surface oil streak flow visualization experiment. These oil streaks agree quite well qualitatively with the computational near wall velocity vectors. Although not shown here, experimental measurements have just been made of flow direction in the duct exit plane. Efforts are currently underway to compare those results with the corresponding three-dimensional PNS computations. Future experiments will include detailed probing of the flow field within this duct and others, and direct measurement of surface shear stress using an advanced laser measurement technique.

In addition to conducting aerodynamic experiments with the highly three-dimensional flow fields of transition ducts, heat-transfer experiments are also being conducted. Heat transfer is of particular concern for these types of flow fields because of applications where the three-dimensional flows may result in high-temperature flow streams (i.e., engine core flow) finding their way to the transition duct (nozzle) surfaces. Figure 8 shows a square-to-rectangular transition duct model which was tested in the facility shown on the right (ref. 4). To measure the surface heat-transfer characteristics of the

duct, the surface was coated with a liquid-crystal material. After establishing the desired amount of airflow through the duct, the duct surface was heated so that the resulting color bands (isotherms) on the liquid-crystal surface could be interpreted in terms of local heat transfer coefficient (refs. 5 to 7).

Results from the liquid-crystal heat-transfer experiment are illustrated in figure 9. Different colors on the liquid-crystal surface correspond to different surface temperatures, which, when combined with the known level of surface heat input, lead to experimentally determined values of surface heat-transfer coefficient. Regions of high and low heat transfer are pointed out in the figure. By photographing the surface and then digitizing the photographic image, quantitative values of surface heat-transfer coefficient are obtained over the entire surface.

SHOCK - BOUNDARY-LAYER INTERACTIONS

Normal Shock - Boundary-Layer Interaction

Shock - boundary-layer interaction research is illustrated by describing the normal shock - boundary-layer interaction research program. Other shock - boundary-layer interaction work is described in references 8 to 12.

Figure 10 illustrates the nature of the normal shock - boundary-layer interaction. The interaction is shown at two Mach numbers, 1.3 and 1.6, and the nature of the interaction is illustrated with a schlieren photograph and a surface oil streak photograph at each Mach number. The photographs were obtained in the Lewis 1- by 1-Foot Supersonic Wind Tunnel. The schlieren photographs give a view of the interaction integrated across the full width of the test section, while the surface oil streaks illustrate the details of the flow field along the sidewall of the test section. At both Mach numbers, the schlieren photographs show the shock being bifurcated into a "lambda shock" in the interacting region. The sidewall surface oil streaks indicate a significant difference in the structure of the flow field for the two cases. At Mach 1.3 the flow along the sidewall remains uniform and passes through the shock structure with no major alteration. At Mach 1.6, the adverse pressure gradient across the shock is strong enough to force the boundary layer to separate from the tunnel walls and form the closed separation bubble shown in the figure. Note that this is a two-dimensional slice through a highly three-dimensional flow field that exists in the corner region.

Both the Mach 1.3 and 1.6 shock - boundary-layer interaction flow fields were surveyed in detail using nonintrusive laser anemometry (ref. 13). Results are shown in figure 11 for the Mach 1.6 case in two different planes within the flow field. The top set of Mach contours illustrates the nature of the flow field in a cross plane downstream of the shock. The lower set of Mach contours shows the development of the flow field within a vertical plane passing through the centerline of the test section. The separated region in the vicinity of the initial interaction causes the actual flow area to contract downstream of the initial shock, leading to a reacceleration of the flow to supersonic Mach numbers. The flow then shocks down again, reaccelerates again because of the thickened boundary layer, and finally shocks down one last time.

In the lower portion of figure 12, the lower portion of figure 11 is repeated, that is, Mach contours as measured with laser anemometry in a vertical plane passing through the centerline of the test section at Mach 1.6. The upper portion of figure 12 is a two-dimensional Navier-Stokes computation of the same flow field. Although the computation captures fairly well the initial portions of the flow in the vicinity of the first shock, in the downstream regions, none of the flow physics are adequately represented in the computation. This result is expected, of course, since the experimental results have shown the strong three-dimensional character of the flow. This comparison points out the need for three-dimensional computational methods for computing such flow fields.

Figure 13 is a frame from a film that illustrates the additional insight and understanding that can be obtained from setting in motion a three-dimensional contour representation of the flow field. The graphics package used to generate the film was actually developed for presenting computational results. The experimental laser anemometry data sets were modified to a format that was acceptable to the graphics software. The researcher can rotate the image, adjust the rate of rotation, and select the axis of rotation while sitting at the display console. One gains a perspective from these rotating images much more quickly than one would by looking at a series of two-dimensional or even three-dimensional plots.

SHEAR LAYER CONTROL

Vortex Generators

The first aspect of shear layer control, boundary layer control, is illustrated by describing the vortex generator research program.

Figure 14 illustrates a research model and facility that were used in an experiment to assess the performance of vortex generators in a diffusing offset duct (ref. 14). The duct had a length-to-diameter ratio of 5.0, an offset-to-diameter ratio of 1.34, and an exit-to-inlet area ratio of 1.50. Initial experiments with the duct identified the location of a separated flow region as shown by the surface oil streak photograph. Vortex generators were then added to the duct surface just upstream of the separated region to control the separation.

A comparison of total pressure contours at various locations down the length of the duct with the vortex generators in place is shown in figure 15. The experimental data were obtained by surveying the flow field with a total pressure probe. The computational results are from the three-dimensional PNS method. The method includes a model for the vortex generators that allows one to position the individual generators anywhere within the duct and permits an adjustment to the strength of the vortex based on an empirical relationship with the vortex generator angle of attack (ref. 15).

Enhanced Jet Mixing

Another aspect of the shear layer control, the use of aerodynamic excitation to control the development and evolution of large-scale structures in a

shear layer, is illustrated by describing the enhanced jet mixing research program. Other shear layer control work, using aerodynamic excitation, is described in references 16 to 31.

The mixing process between a jet and the surrounding air flow can be enhanced through use of aerodynamic excitation as illustrated in figure 16. The naturally occurring flow structure of the jet mixing process is shown in the left-hand schlieren photograph. By applying an excitation signal at the proper frequency, here by use of acoustic drivers upstream of the jet exit plane, the naturally occurring large-scale structures within the mixing layer are regularized and enhanced and lead to a more rapid mixing process as illustrated in the right-hand photograph.

Results of an axisymmetric Navier-Stokes computation of a jet flow exiting into a quiescent region are shown in figure 17 (ref. 32). The jet exit Mach number is 0.3, and the results are shown in terms of vorticity contours. Two cases are shown - an unexcited case on the left side, and an excited case on the right side. For the excited case, the excitation signal is applied at a frequency chosen to maximize the development and growth of the large-scale structures. In both cases, results of the computation are shown at three different times. Also for both cases, lines are drawn through the centers of the large-scale vortices to illustrate how they propagate downstream. Note that with excitation applied at the proper frequency, adjacent vortices combine or pair to form a single larger vortex, which, in turn, has the effect of more rapidly mixing the jet flow with the surrounding quiescent flow.

The effect of excitation on the jet mixing process for a jet having an exit Mach number of 0.3 and an initial turbulence level of 0.15 percent is shown in figure 18. The results were obtained in an experiment wherein both the frequency and the level of the excitation signal could be varied (ref. 33). The results show how the ratio of centerline velocity for the excited case to that of the unexcited case varies as the level of the excitation is increased at a fixed frequency. The measurements are made nine jet diameters downstream of the nozzle exit plane. As in the previous figure, the excitation frequency has been selected to provide the maximum degree of mixing enhancement. As indicated, the effect of the excitation is quite significant with, in this case, a reduction in centerline velocity of about 16 percent at the maximum available excitation level of 130 dB.

The internal fluid mechanics research program in inlets, ducts, and nozzles is a balanced effort between the development of computational tools and the conduct of experimental research. The program has been briefly described by highlighting research efforts in highly three-dimensional flow fields, shock - boundary-layer interactions, and shear layer control. Much of the computational focus up until now has been on the development and validation of parabolized Navier-Stokes methods. More recently, and in the future, more emphasis will be placed on the development and validation of three-dimensional Navier-Stokes methods. The experimental element of the program will continue to provide a fundamental understanding of the fluid flow physics, develop new and/or improved flow models, and to provide benchmark data sets for computational method validation of both the parabolized and full Navier-Stokes methods.

REFERENCES

1. Patrick, W.P.; and McCormick, D.C.: Circular-to-Rectangular Duct Flows, A Benchmark Experimental Study. SAE Paper 871776, Oct. 1987.

2. Briley, W.R.; and McDonald, H.: Analysis and Computation of Viscous Subsonic Primary and Secondary Flows. AIAA Paper 79-1453, July 1979.

3. Briley, W.R.; and McDonald, H.: Three-Dimensional Viscous Flows With Large Secondary Velocity. J. Fluid Mech., vol. 144, July 1984, pp. 47-77.

4. Jones, T.V.; and Hippensteele, S.A.: High-Resolution Heat-Transfer-Coefficient Maps Applicable to Compound-Curve Surfaces Using Liquid Crystals in a Transient Wind Tunnel. Developments in Experimental Techniques in Heat Transfer and Combustion, R.O. Warrington, Jr., M.M. Chen, and J.D. Felske, eds., ASME, 1987, pp. 1-9.

5. Hippensteele, S.A.; Russell, L.M.; and Stepka, F.S.: Evaluation of a Method for Heat Transfer Measurements and Thermal Visualization Using a Composite of a Heater Element and Liquid Crystals. ASME Paper 81-GT-93, Mar. 1981 (NASA TM-81639).

6. Hippensteele, S.A.; Russell, L.M.; and Torres, F.J.: Local Heat-Transfer Measurements on a Large, Scale-Model Turbine Blade Airfoil Using a Composite of a Heater Element and Liquid Crystals. NASA TM-86900, 1985.

7. Hippensteele, S.A.; Russell, L.M.; and Torres, F.J.: Use of a Liquid-Crystal, Heater-Element Composite for Quantitative, High-Resolution Heat Transfer Coefficients on a Turbine Airfoil, Including Turbulence and Surface Roughness Effects. NASA TM-87355, 1987.

8. Hingst, W.R.; and Tanji, F.T.: Experimental Investigation of a Two-Dimensional Shock-Turbulent Boundary Layer Interaction with Bleed. AIAA Paper 83-0135, Jan. 1983 (NASA TM-83057).

9. Jurkovich, M.S.: Flow Visualization Studies of 3-D Shock/Boundary-Layer Interaction in the Presence of a Non-Uniform Approach Boundary Layer. AIAA Paper 84-1560, June 1984.

10. Skebe, S.A.; Greber, I.; and Hingst, W.R.: Investigation of Two-Dimensional Shock-Wave/Boundary-Layer Interactions. AIAA J., vol. 25, no. 6, June 1987, pp. 777-783.

11. Barnhart, P.J.; Greber, I.; and Hingst, W.R.: Glancing Shock Wave-Turbulent Boundary Layer Interaction with Boundary Layer Suction. AIAA Paper 88-0308, Jan. 1988.

12. Benhachmi, D.; Greber, I.; and Hingst, W.R.: Experimental and Numerical Investigation of the Effect of Distributed Suction on Oblique Shock Wave/Turbulent Boundary Layer Interaction. NASA TM-101334, 1988.

13. Chriss, R.M., et al.: An LDA Investigation of Three-Dimensional Normal Shock-Boundary Layer Interactions in a Corner. AIAA Paper 87-1369, June 1987.

14. Vakili, A.D., et al.: Flow Control in a Diffusing S-Duct. AIAA Paper 85-0524, Mar. 1985.

15. Kunik, W.G.: Application of a Computational Model for Vortex Generators in Subsonic Internal Flows. AIAA Paper 86-1458, June 1986.

16. Stone, J.R.; and McKinzie, D.J., Jr.: Acoustic Excitation - A Promising New Means of Controlling Shear Layers. NASA TM-83772, 1984.

17. Rice, E.J.; and Zaman, K.B.M.Q.: Control of Shear Flows by Artificial Excitation. AIAA Paper 87-2722, Oct. 1987.

18. Lepicovsky, J., et al.: Acoustically Excited Heated Jets. I-Internal Excitation, II-In Search of a Better Understanding, III-Mean Flow Data, NASA CR-4129-PT-1,-2,-3, 1988.

19. Zaman, K.B.M.Q.; Bar-Sever, A.; and Mangalam, S.M.: Effect of Acoustic Excitation on the Flow Over a Low-Re Airfoil. J. Fluid Mech., vol. 182, Sept. 1987, pp. 127-148.

20. Mangalam, S.M., et al.: Transition and Separation Control on a Low-Reynolds Number Airfoil. Aerodynamics at Low Reynolds Numbers Re Greater Than 10^4 and Less Than 10^6, Vol. 1, Royal Aeronautical Society, London, 1986, pp. 10.1-10.19.

21. Raman, G.; Ghorashi, B.; Rice, E.J.; and Miles, J.H.: Enhanced Mixing in Free Shear Layers by Acoustic Excitation. Presented at the AIChE Annual Meeting, Nov. 10-15, 1985.

22. Raman, G.: Enhanced Mixing of an Axisymmetric Jet by Aerodynamic Excitation. NASA CR-175059, 1986.

23. Ghorashi, B.; Raman, G.; Rice, E.J.; and Miles, J.H.: Upstream Excitation of an Axisymmetric Jet. Presented at the AIChE Annual Meeting, Miami, FL, Nov. 3-7, 1986.

24. Ghorashi, B.; and Raman, G.: Measurements in an Acoustically Excited Jet. Proceedings of the 4th Miami International Symposium on Multi-Phase Transport and Particulate Phenomena, Clean Energy Research Institute, University of Miami, Coral Gables, FL, Dec. 15-17, 1986.

25. Raman, G.; Rice, E.J.; and Mankbadi, R.R.: Saturation and the Limit of Jet Mixing Enhancement by Single Frequency Plane Wave Excitation: Experiment and Theory. National Fluid Dynamics Congress, 1st, Pt. 2, AIAA, 1988, pp. 1000-1007 (NASA TM-100882).

26. Raman, G.; Zaman, K.B.M.Q.; and Rice, E.J.: Controlled Excitation of a Round Jet at Various Levels of Initial Turbulence. Bull. Am. Phys. Soc., Division of Fluid Dynamics, Nov. 23-25, 1986.

27. Raman, G.; and Rice, E.J.: Excitation of an Axisymmetric Jet at Fundamental and Subharmonic Frequencies. Presented at the 41st Annual Meeting of the American Physical Society, Nov. 20-22, 1988.

28. Mankbadi, R.R.; Raman, G.; and Rice E.J.: Effects of Core Turbulence on Jet Excitability. Presented at the 41st Annual Meeting of the American Physical Society, Nov. 20-22, 1988.

29. Taghavi, R.; Rice, E.J.; and Farokhi, S.: Controlled Excitation of a Cold Turbulent Swirling Free Jet. J. Vibration, Acoustics, Stress, Reliability Design, vol. 110, no. 2, Apr. 1988, pp. 234-237.

30. Farokhi, S.; Taghavi, R.; and Rice E.J.: Effect of Initial Tangential Velocity Distribution on the Mean Evolution of a Swirling Turbulent Free Jet. National Fluid Dynamics Congress, 1st, Pt. 2, AIAA, 1988, pp. 947-954 (NASA TM-100934).

31. Taghavi, R.; and Farokhi, S.: Turbulent Swirling Jets With Excitation, NASA CR-180895, 1988.

32. Scott, J.N.: Numerical Simulation of Self-Sustained and Forced Oscillations in Jet Shear Layers. Forum on Unsteady Flow Separation, K.N. Ghia, ed., ASME 1987, pp. 123-130.

33. Raman, G.; Zaman, K.B.M.Q.; and Rice, E.J.: Initial Turbulence Effects on Jet Evolution With and Without Tonal Excitation. AIAA Paper 87-2725, Oct. 1987 (NASA TM-100178).

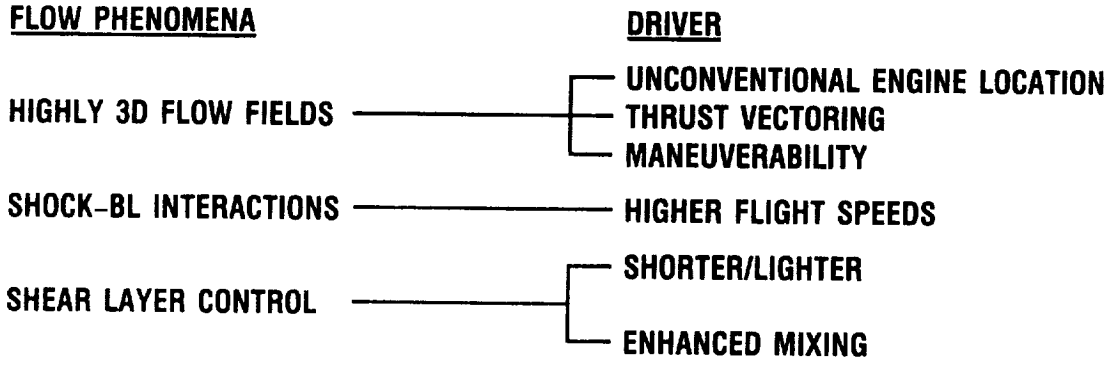

Figure 1. - Flow phenomena of interest in inlets, ducts, and nozzles together with interest drivers.

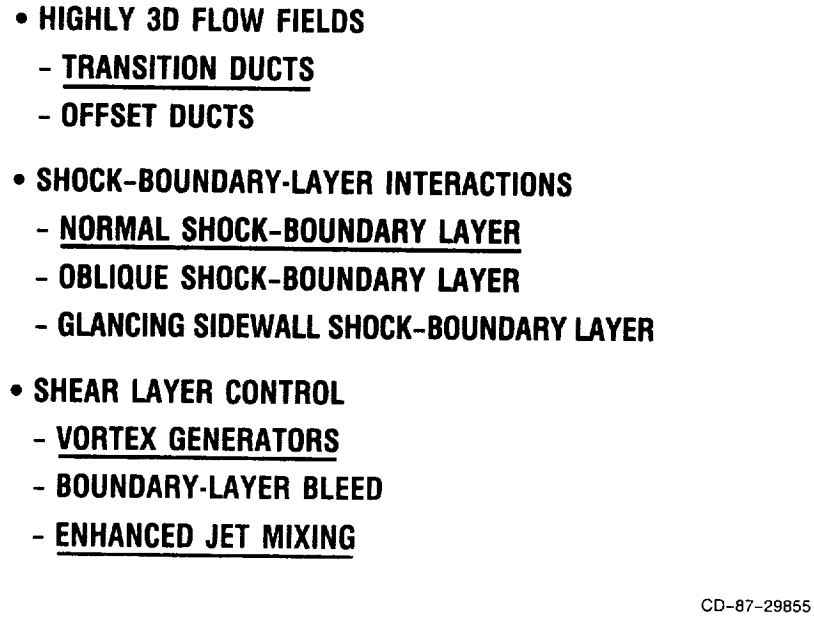

Figure 2. - Elements of inlet, duct, and nozzle research program.

COMPUTATIONAL METHODS	EXPERIMENTS
3D PARABOLIZED NAVIER-STOKES (PNS)	(1) TRANSITION DUCTS (2) OFFSET DUCTS (3) SHOCK-BOUNDARY-LAYER INTERACTION (4) VORTEX GENERATORS (5) BOUNDARY-LAYER BLEED
3D NAVIER-STOKES (NS)	(6) EXPERIMENTS (1) TO (5) (7) SEPARATION FLOW PHYSICS (8) NONORTHOGONAL SURFACES (9) JET MIXING

CD-87-29856

Figure 3. - Approach to research program in inlets, ducts, and nozzles.

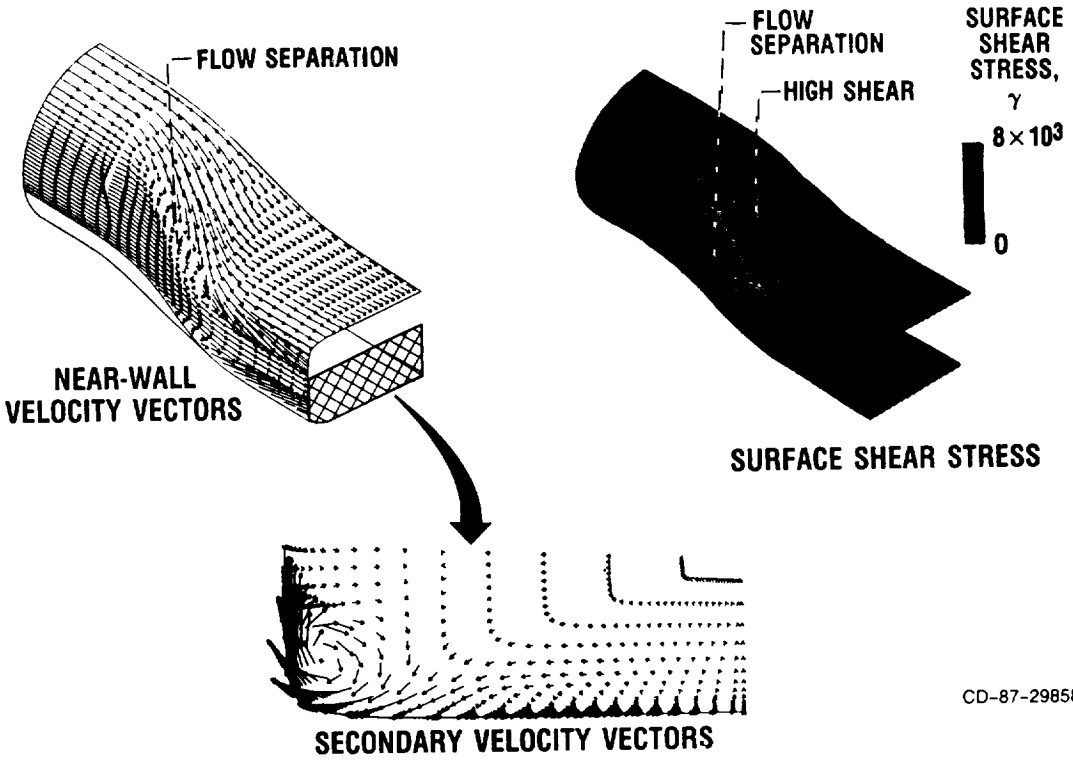

Figure 4. - Three-dimensional PNS computational results for transition duct (duct exit aspect ratio (width/height), 3.0; duct length to inlet diameter ratio, 1.5; duct exit-to-inlet area ratio, 1.0).

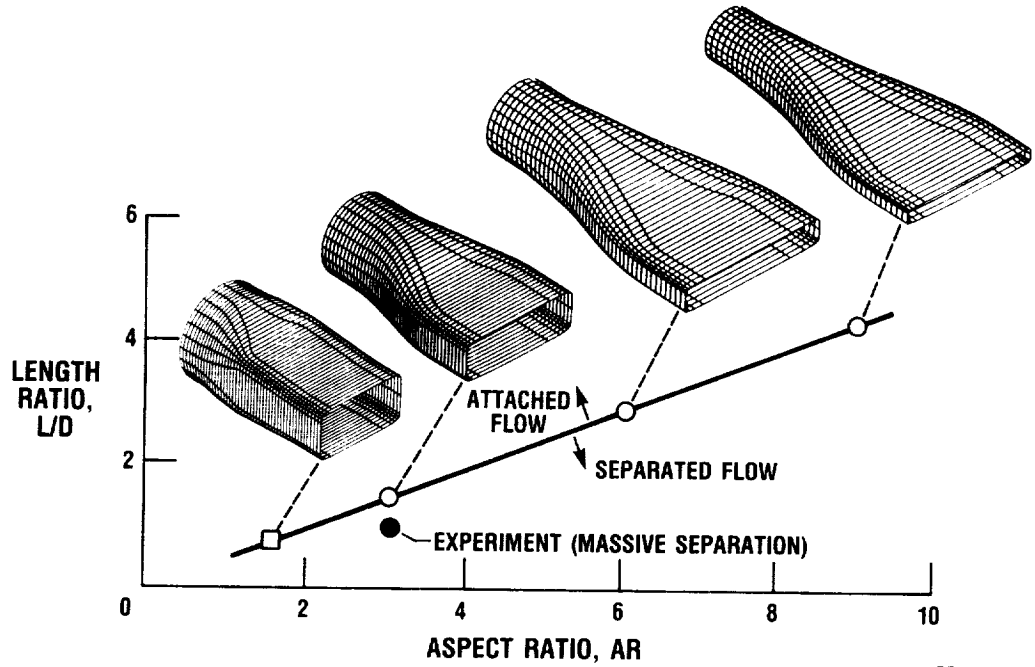

Figure 5. - Three-dimensional PNS computations of transition duct separation characteristics (transition duct exit-to-inlet area ratio, 1.0).

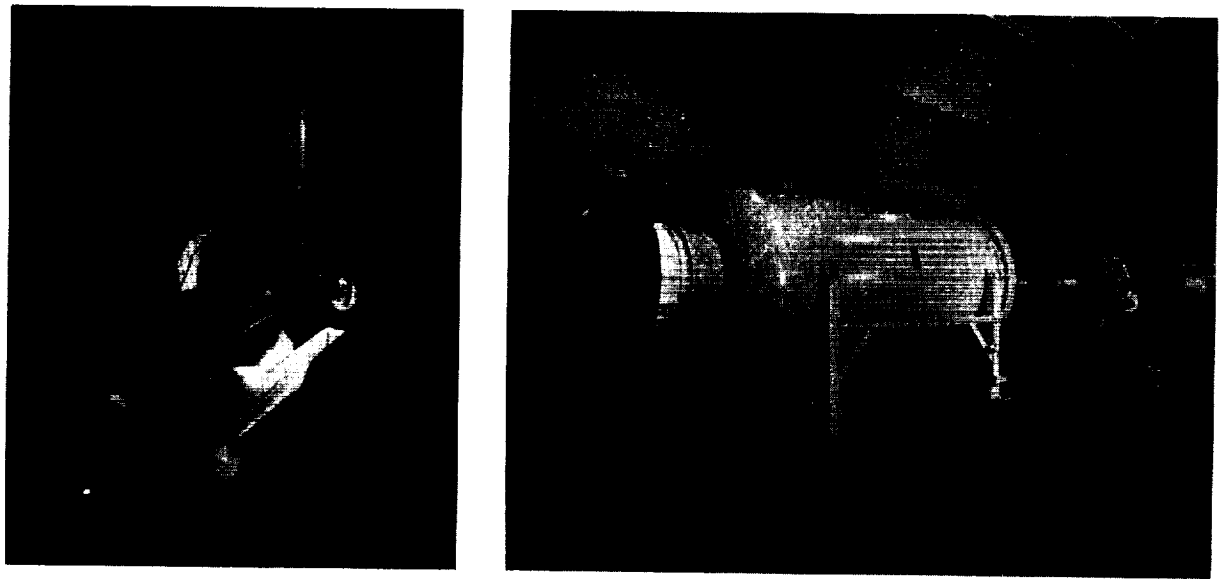

Figure 6. - Transition duct aerodynamic experiments.

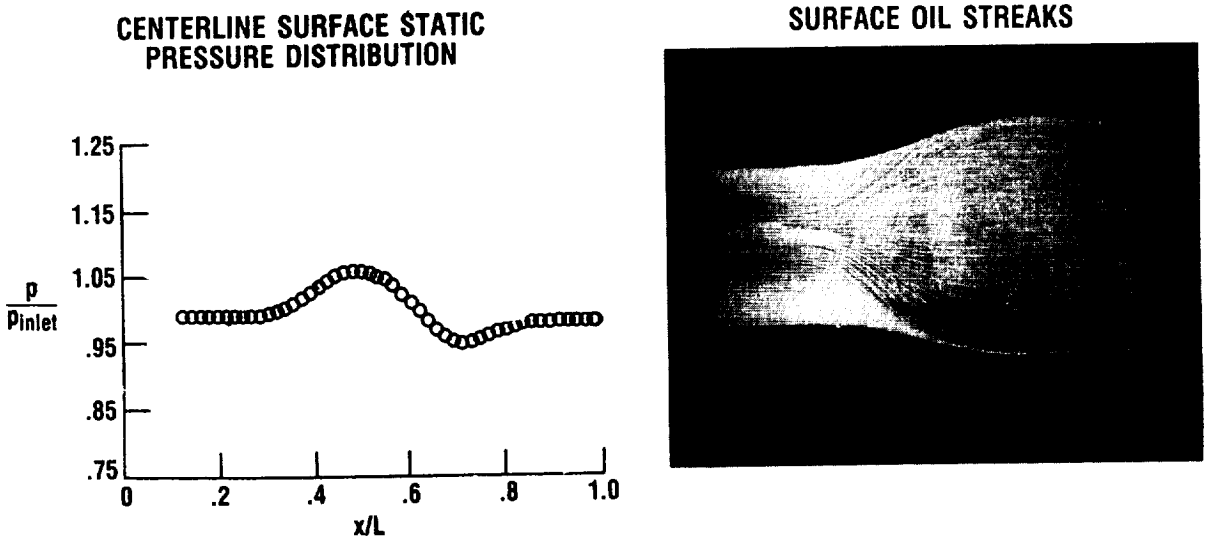

Figure 7. - Transition duct aerodynamic results (duct Mach number, 0.5).

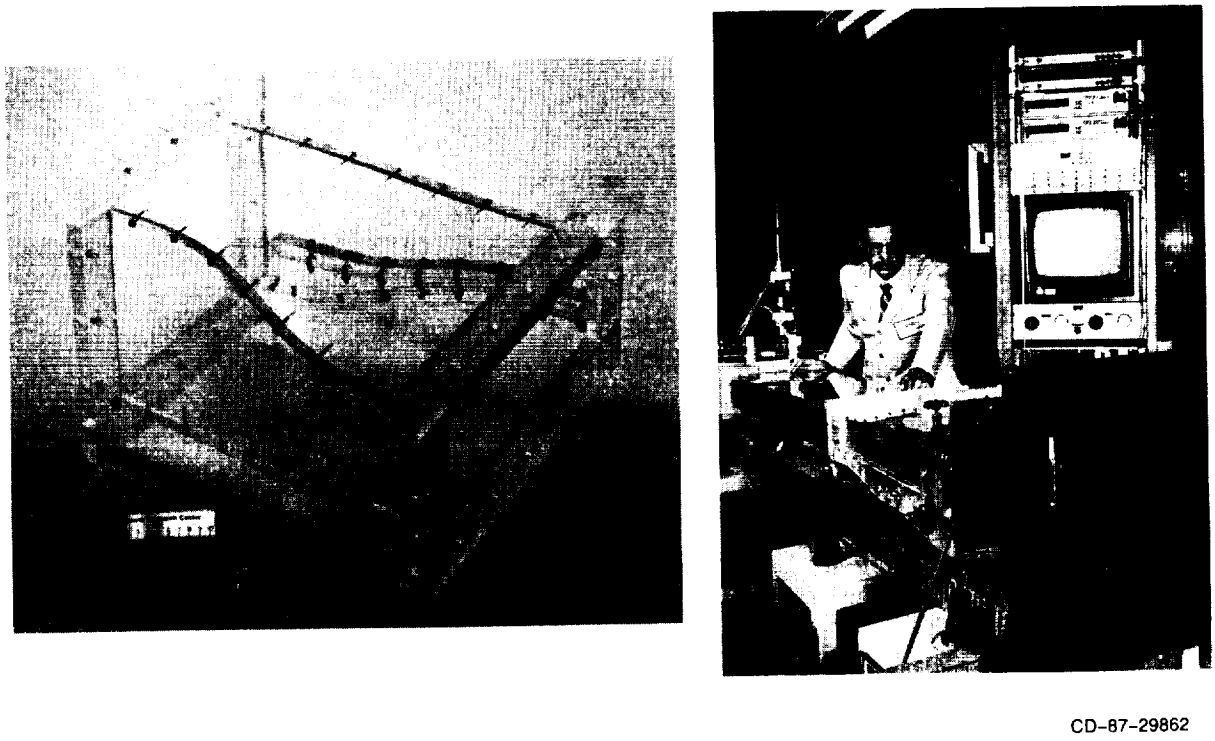

Figure 8. - Transition duct heat-transfer experiments.

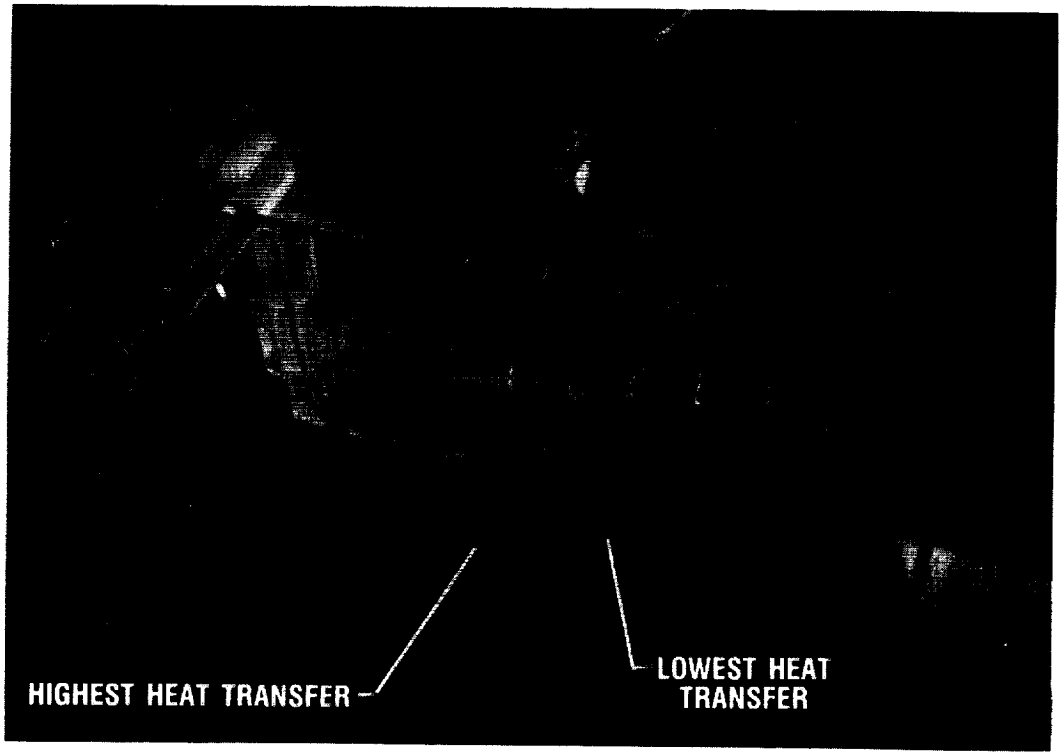

CD-87-29863

Figure 9. - Transition duct heat-transfer results.

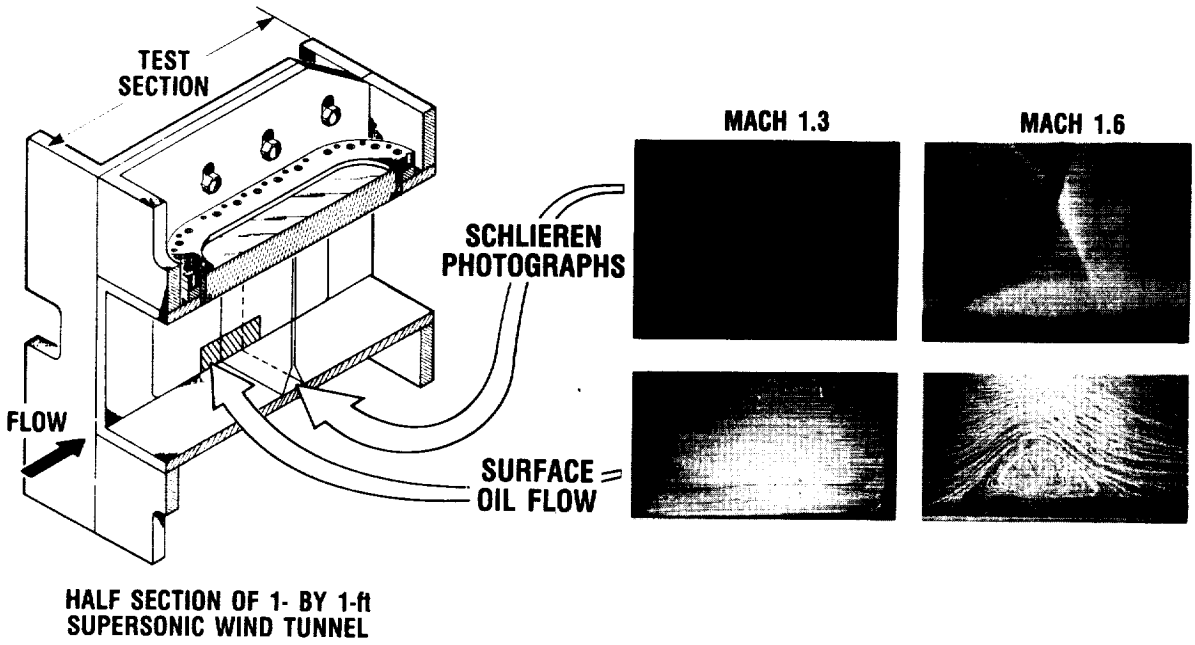

CD-87-29864

Figure 10. - Normal shock - boundary-layer interaction experiments.

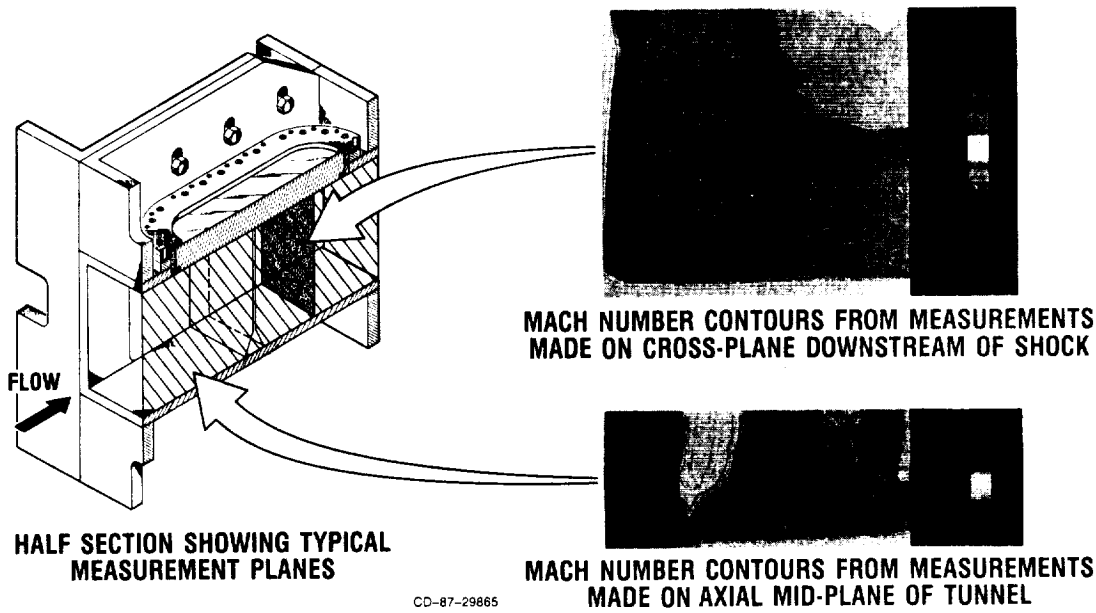

Figure 11. - Results of laser anemometer measurements for normal shock - boundary-layer interaction at Mach 1.6.

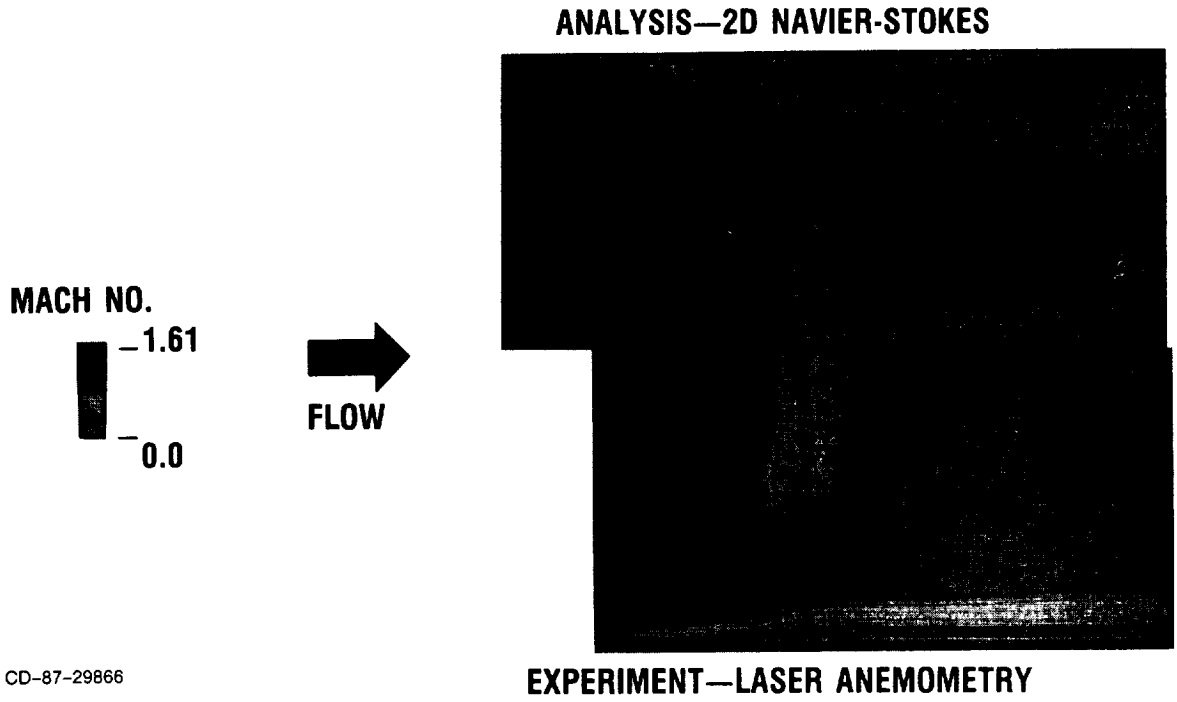

Figure 12. - Comparison of LDV experiment and two-dimensional Navier-Stokes calculation for Mach 1.6 normal shock - boundary-layer interaction.

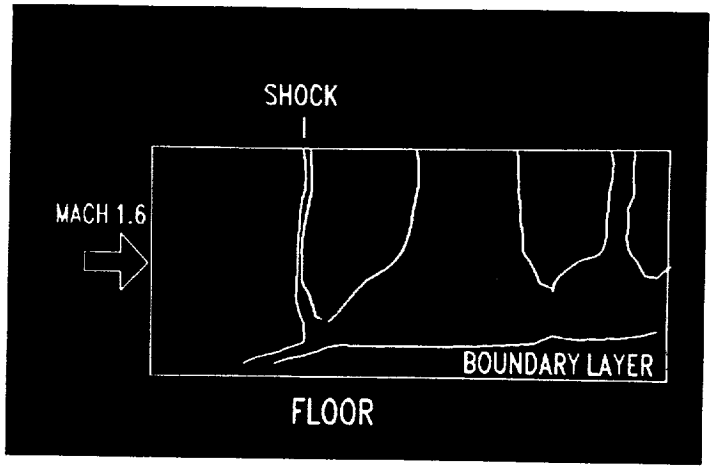

CD-87-29867

Figure 13. - Frame from film showing laser anemometry results of normal shock - boundary-layer interaction.

EXPERIMENT SETUP

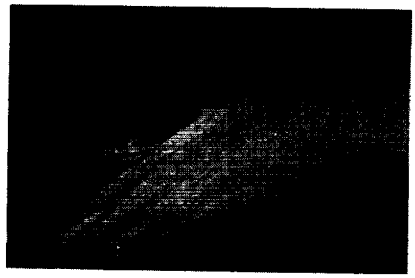

SURFACE OIL STREAKS
WITHOUT VORTEX GENERATORS

VORTEX GENERATORS

CD-87-29868

Figure 14. - Vortex generators in diffusing offset duct (duct length-to-diameter ratio, 5.0; duct offset-to-diameter ratio, 1.34; duct exit-to-inlet area ratio, 1.50).

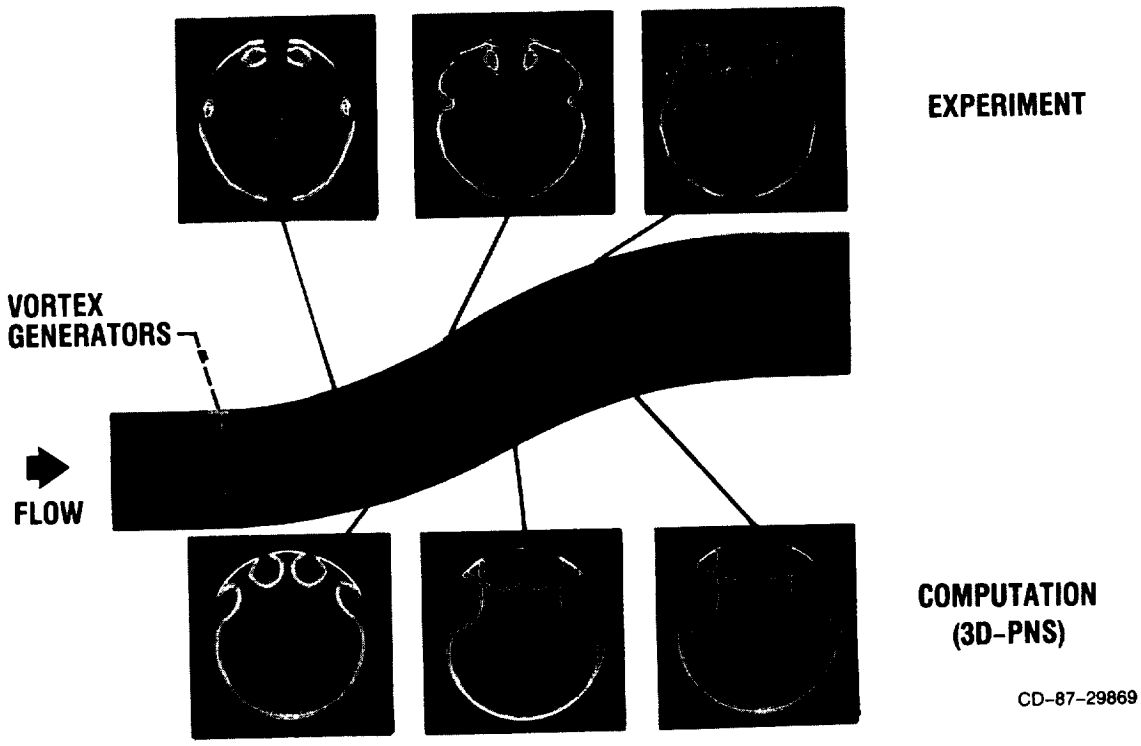

Figure 15. - Comparison of analysis and experiment for vortex generators in diffusing offset duct (total pressure contours at duct Mach number of 0.6).

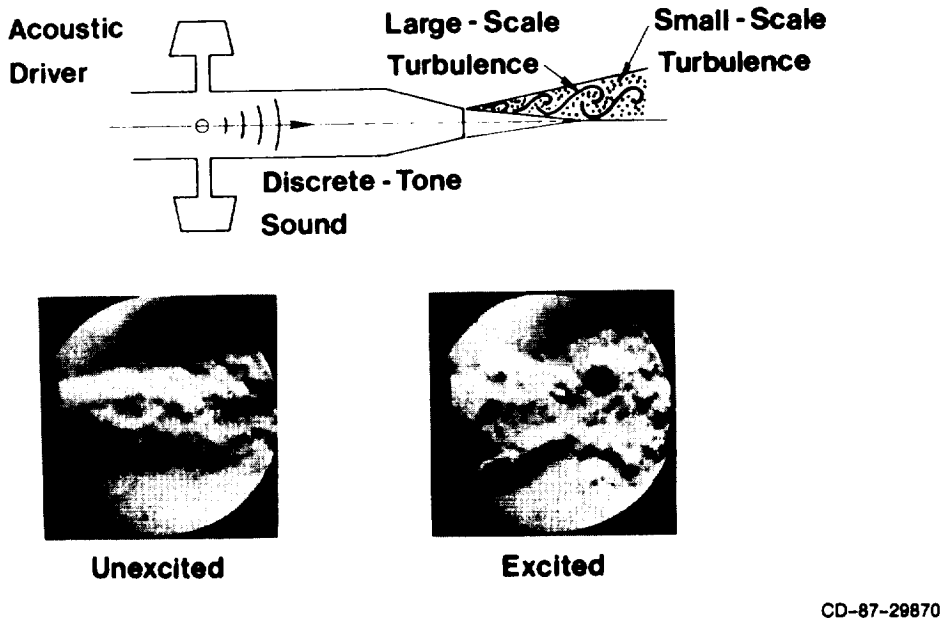

Figure 16. - Enhanced jet mixing through excitation of coherent large-scale turbulence.

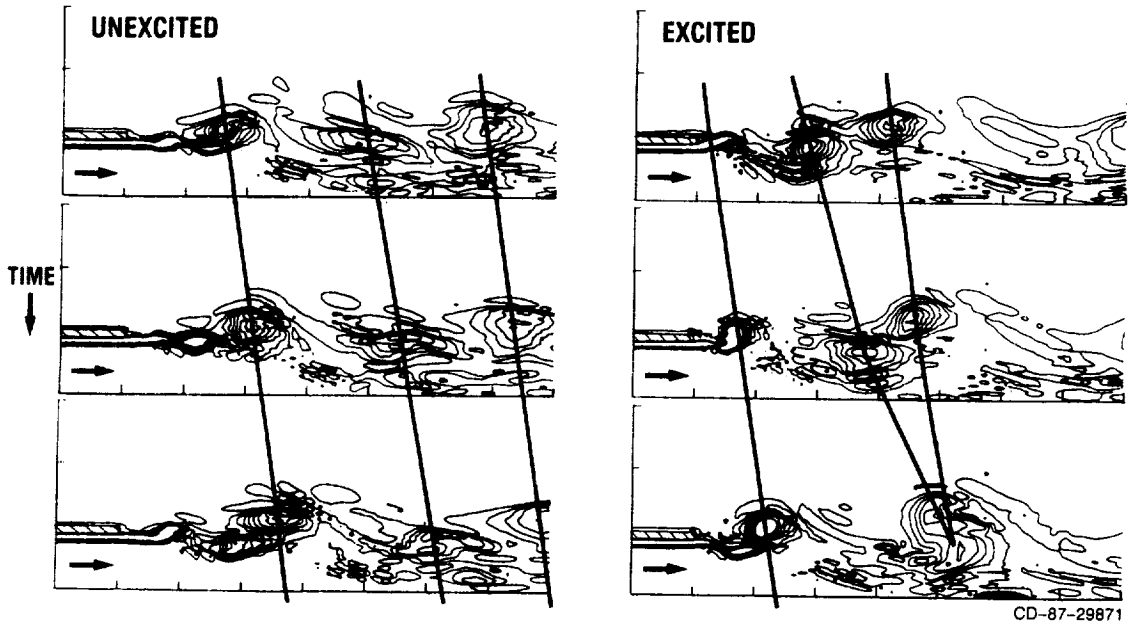

Figure 17. - Navier-Stokes computational results showing effect of excitation on jet shear layer evolution (vorticity contours at jet Mach number of 0.3).

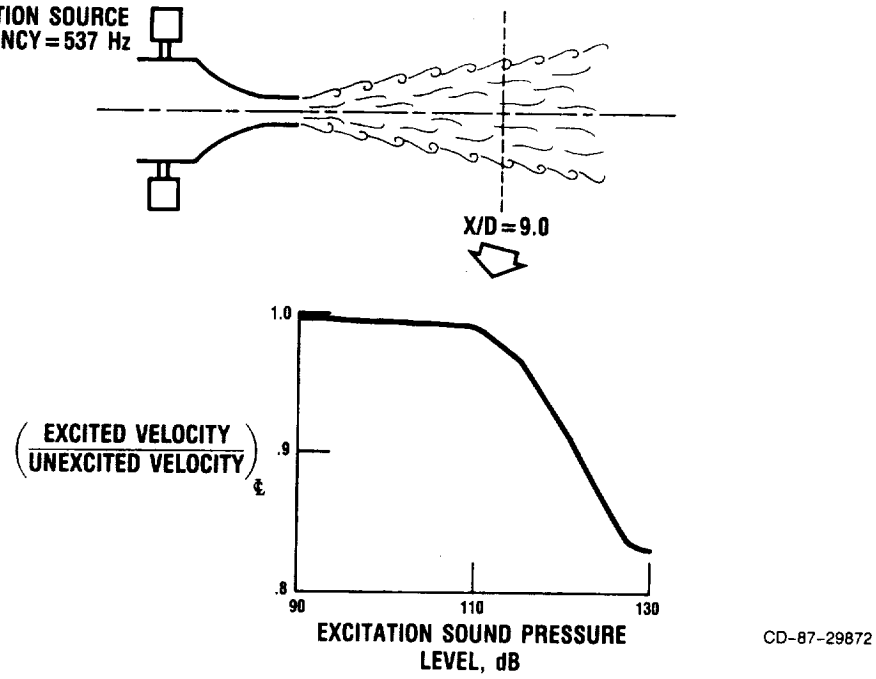

Figure 18. - Experimental results showing effect of excitation on jet mixing (jet exit Mach number, 0.3; jet exit turbulence, 0.15 percent).